

# Steering the receiving field of view (FOV) without applying delays in synthetic transmit aperture imaging (STA)

Ying Li, Michael C. Kolios, and Yuan Xu\*

Department of Physics, Ryerson University

Institute for Biomedical Engineering, Science and Technology (iBEST), a partnership between Ryerson University and St. Michael's Hospital

Keenan Research Centre for Biomedical Science of St. Michael's Hospital  
Toronto, Canada

\*[yxu@ryerson.ca](mailto:yxu@ryerson.ca)

**Abstract**— This paper presents an approach to steer the receiving field of view (FOV) of ultrasound imaging by linearly combining the RF signals from adjacent elements of a phased array without applying delay to the elements. The motivation is to reduce the number of measurement channels  $M$  (the product of number of transmissions,  $n_T$ , and the number of receiving channels in each transmission,  $n_R$ ) while retaining the steering ability of a phased array. To reduce  $M$ , adjacent transducer elements were combined into groups by applying proper delays in transmission and weighting function in receiving to steer the FOV. After the  $M$  channels of RF data were acquired, a conjugate transpose was applied to estimate the equivalent signal in the traditional synthetic transmit aperture imaging (STA) to reconstruct a STA image. We reported the results in the case with  $M=N^2/66$ , where  $N$  is the number of the array elements. The proposed system has potential applications in 3D ultrasound imaging.

**Keywords**—spatially encoding, elements combination, beam steering

## I. INTRODUCTION

To avoid the grating lobe artifacts, the inter-element spacing of the array has to be less than half a wavelength [1]. When using the fully-addressed 2D array in transmit and receive for 3D ultrasound imaging, the number of active channels is large and therefore the cost of the hardware system will be prohibitively high due to the digital electronics associated with each element [2]. Many innovations in designing sparse arrays have been investigated [3]-[11]. Lockwood *et al.* [5] proposed a framework of designing sparse arrays by using the effective aperture concept. The two-way radiation pattern of a sparse array can be optimized to reduce the grating lobe artifacts by arranging the element spacing properly. However, grating lobes still affect the image quality when using a periodic sparse array. Random sparse arrays can also suffer from the significant side lobes [12]. Furthermore, the coherent array imaging method [13] with the subarray techniques was proposed to reduce the number of coaxial cables in an array probe. In this design, the subarray aperture moved across the entire array to achieve an improved lateral

resolution at the cost of a decreased frame rate and a worse SNR.

In addition to sparse arrays, Liu proposed a solution by changing the element spacing of transmit and receive by joining the elements into groups to reduce the negative effects of grating lobes [4]. Even though such a system costs less than a fully-sampled phased array system, the steering and focusing of the linear array is usually restricted along the forward direction (perpendicular to the transducer array) [14]. An earlier publication [15] by the authors investigated whether specific combination schemes can be selected following the effective aperture concept [5] to suppress the grating lobe level of the two-way radiation pattern. As shown in [15], adjusting the delay for both transmit and receive can steer the limited FOV in the large-pitch linear array system. In the receiving process of the real-time system, it is possible to combine the signals from adjacent elements after applying proper delays as shown in the micro-beamforming technique [16]. However, the fabrication process of such design is still complex. In this paper, we propose to apply receiving encoding patterns (REP) to the receive elements to steer the FOV without adjusting the delay for the receive elements.

In Section II, the theory of the proposed method will be presented. The implementation of the method will be described and the simulation parameters stated. Image quality metrics will be applied to the reconstructed images. In Section III, the image quality of the simulated images from the proposed method will be assessed and compared to the standard STA. The discussion and conclusion will be presented in Section IV.

## II. METHODS

### A. Encoding and decoding processes

Generally, we assume there are  $N$  elements in the transducer array, and  $L$  transmissions to acquire one frame. A transmission encoding matrix  $\mathbf{T}$  with the size of  $L$ -by- $N$  is defined in a similar format as in [15]. We can define  $\mathbf{R}$  as an  $N$  by  $K$  matrix to encode the receiving elements in a similar way,

where  $K$  is the number of receiving groups/channels. In each transmission, one group of transmitters will transmit a wave, and all the receiving groups will be used to receive the signals. The encoding processes in both transmit and receive can be described as

$$\mathbf{T}\mathbf{S}(t)\mathbf{R} = \mathbf{M}(t), \quad (1)$$

where  $\mathbf{S}(t)$  is the equivalent traditional STA signal matrix with a size  $N$  by  $N$  from a fully-sampled phased array system, and  $S_{ij}(t)$  is the signal for time  $t$  transmits at  $i$ -th element and received by the  $j$ -th element.  $\mathbf{M}(t)$  is a measurement matrix from the large-pitch array system, and  $M_{ij}(t)$  is the signal at time  $t$  when the  $i$ -th group transmits and the  $j$ -th group receives.

The transmission and receiving encoding processes could be combined by using a mathematical identity of the Kronecker product [18] to generate the encoding operator as,

$$\mathbf{E} = \mathbf{R}^T \otimes \mathbf{T}, \quad (2)$$

where the superscript  $T$  means the transpose of the matrix. By combining the Eq. (1) and (2), the encoding operator  $\mathbf{E}$  can be applied to the traditional STA signal. Note that to apply this operator properly, the traditional STA signals  $\mathbf{S}(t)$  and  $\mathbf{M}(t)$  have to be vectorized into column vectors  $\mathbf{S}_{vector}(t)$  and  $\mathbf{M}_{vector}(t)$  by stacking the columns of the corresponding matrix, respectively. We have

$$\mathbf{E}\mathbf{S}_{vector}(t) = \mathbf{M}_{vector}(t), \quad (3)$$

In the decoding process, to recover  $\mathbf{S}$  from  $\mathbf{M}$ , pseudo-inversion with regularization can be used. When a delay was applied to the encoding process, the above equation can be transformed into the frequency domain, in which each frequency component can be decoded separately [17]. However, the frequency-domain pseudo-inversion was time-consuming due to the large size of the RF signals. Therefore, we used the conjugate transpose of the encoding operator  $\mathbf{E}$  to approximate the pseudo-inversion to simplify and accelerate the decoding process. After acquiring the traditional STA RF signal, the standard delay-and-sum (DAS) algorithm was used to obtain the reconstructed images.

### B. Encoding schemes without steering FOV

In this section, we will use the case without steering FOV, in which FOV is right underneath the probe, to demonstrate the construction of  $\mathbf{R}$  and  $\mathbf{T}$ . In the transmission mode,  $l$  adjacent elements in one group are combined to be excited by one source with applying proper delay to each element within each group to steer the FOV to any desired angle. For example,  $l=6$  represents six elements combined as one group to produce one transmission. The first group includes the elements from the first one to the sixth one. If  $N/l$  is not an integer, in the last group there are  $(l+\text{mod}(N, l))$  ( $\text{mod}$  represents the modulo function) elements combined together. The transmission-encoding matrix  $\mathbf{T}$  can be written as,

$$\mathbf{T} = \mathbf{I}_{N/l} \otimes \mathbf{V}_l^T, \quad (4)$$

where  $\mathbf{I}$  is the identity matrix with the size of  $N/l$ . Therefore, the number of transmissions can be reduced to  $N/l$ . Generally,  $\mathbf{V}_l$  is an  $l$ -order column vector. In the case with no steering,  $\mathbf{V}_l$  is an  $l$ -order column vector with all ones.  $\otimes$  represents the Kronecker product.

In our receiving encoding design,  $k$  adjacent elements are combined together as one receiver ( $k$  can be an arbitrary integer). The signal from this group receiver is the summation of the signals from the  $k$  elements by applying proper weighting function (receiving encoding pattern, REP, which will be explained later) to each element to steer the beam to any desired angle. This will reduce the number of receiving channels from  $N$  to about  $N/k$ . Similarly, if  $N/k$  is not an integer, there are  $(k+\text{mod}(N, k))$  elements in the last group. Therefore, the receiving encoding matrix  $\mathbf{R}$  can be defined as

$$\mathbf{R} = \mathbf{I}_{N/k} \otimes \mathbf{V}_k, \quad (5)$$

where  $\mathbf{I}$  is the identity matrix with the size of  $N/k$ .  $\mathbf{V}_k$  is a  $k$ -order column vector. In the case with no steering,  $\mathbf{V}_k$  is a  $k$ -order column vector of all ones. In this paper  $k$  and  $l$  were chosen to be relatively prime to achieve the optimized grating-lobe reduction.

### C. Encoding schemes when steering FOV

In this section, we will explain how to construct  $\mathbf{R}$  and  $\mathbf{T}$  in the case of steering FOV. As mentioned in [15], the disadvantage of the above proposed approach is that its FOV in one delay-configuration is smaller than a standard fully-sampled phased array. Normally in transmission, the time delay,  $d(x)$ , for the element at  $x$  can be adjusted to steer the FOV to a certain steering angle  $\theta_s$ . In this paper, the  $d(x)$  can be represented as,

$$d(x) = \frac{\delta_x \sin(\theta_s)}{c}, \quad (6)$$

where  $\delta_x$  is the distance between the center of the element at  $x$  to the center of that group, and  $c$  is the speed of sound. Note that the delay in Eq. 6 is similar to that in micro-beamforming [16]. The delay is applied to elements in one group and it is the same for the different groups of elements.  $d(x)$  can be used to construct the transmission encoding matrix  $\mathbf{T}$  in the temporal frequency domain by replacing the ones in the  $\mathbf{V}_l$  in Eq. 4 with the corresponding phase factor.

A receiving encoding pattern (REP) can be treated as a weighting function to be applied to the receiving elements in each receive group. REP will replace  $\mathbf{V}_k$  in Eq. 5 to construct  $\mathbf{R}$ . Similar to the apodization theory on an ultrasound probe, the Fourier transform of REP is related to the beam pattern of the probe in the far field of the probe. To steer the FOV to  $\theta_s$ , the REP can be expressed as

$$\text{REP}(n) = \sin\left(\frac{2\pi pn}{m\lambda} + \varphi\right), n = 1, 2, \dots, k, \quad (7)$$

where  $m = 1/\sin(\theta_s)$ ,  $\lambda$  is the wavelength at the central frequency of the probe,  $p$  denotes the pitch of the probe, and  $n$  represents  $n$ -th element in a group. We also introduced a shifting factor  $\varphi$  to ensure that the summation of each REP equals to zero, which is not always true when  $k$  is small. Because the summation of REP is the DC component of REP, which represents the beam strength along the forward direction. If the summation of the pattern equals to zero, the strength of the beam along the forward direction is zero, which is desirable if we want to steer the FOV. Since the Fourier transform of the above REP has a significant value at both a positive frequency and a negative frequency, one REP can generate two steering angles, which are placed symmetric about the axial direction of the probe. This is different from steering by applying delays, in which the beam is steered to only one angle.

#### D. Simulation methods

##### 1) Simulation parameters

The FIELD II program [19] was used to generate the standard STA RF data. The probe was simulated as a 128-element, 2-cm wide, 5-MHz central frequency phased array with a 0.15-mm pitch, 0.01-mm kerf and 10-mm height. The sampling frequency was 40 MHz.

##### 2) Simulation phantoms

There were two simulated phantoms in our simulations with the size of is 6 cm  $\times$  1 cm  $\times$  6 cm (Azimuth  $\times$  Elevational  $\times$  Axial). The first simulation phantom contains twenty-five point targets placed in five rows from top to bottom at 1.5 cm, 2.5 cm, 3.5 cm, 4.5 cm, and 5.5 cm in depth, and apart by 1 cm laterally for each row. The second simulated medium is a medium with background scattering, which includes thirty-five 5-mm-diameter hypo-echoic inclusions placed in five rows from top to bottom, with the rows placed at 1.5 cm, 2.5 cm, 3.5 cm, 4.5 cm, and 5.5 cm depth. For each row, the centers of the middle three hypo-echoic lesions are separate by 6 mm apart horizontally, and the other lesions are placed at 0.5 cm, 1.5 cm, 4.5 cm, and 5.5 cm in the horizontal direction. The simulated probe was located from 2 cm to 4 cm laterally, and 0.5 cm away from the top of the simulated medium. The log-enveloped beamformed images were displayed after applying the Hilbert transform and logarithm compression to the reconstructed images.

#### E. Imaging quality metrics

The contrast to noise ratio (CNR) of inclusions was calculated as:

$$\text{CNR} = \frac{\mu_{\text{lesion}} - \mu_{\text{background}}}{\sqrt{\sigma_{\text{lesion}}^2 + \sigma_{\text{background}}^2}}, \quad (8)$$

where  $\mu_{\text{lesion}}$  and  $\mu_{\text{background}}$  are the mean value of log-enveloped region of lesion and background, respectively, and

$\sigma_{\text{lesion}}$  and  $\sigma_{\text{background}}$  are the standard deviation of the lesion and background, respectively.

### III. RESULTS

Fig. 1 shows the log-enveloped beamformed images obtained from (a) the standard STA, and (b) the configuration with reduced  $M$ ,  $(n_T, n_R) = (N/6, N/11)$ . The bottom row of the figure shows a lateral line plot through the centers of point targets at the depth of 5.5 cm (the central three point targets are plotted for comparison). More artifacts and blurring can be found in the image of  $(N/6, N/11)$  configuration when the target is placed close to the transducer array. However, the artifacts and blurring are reduced with increasing depth, also confirmed by central point target in the lateral line plot.

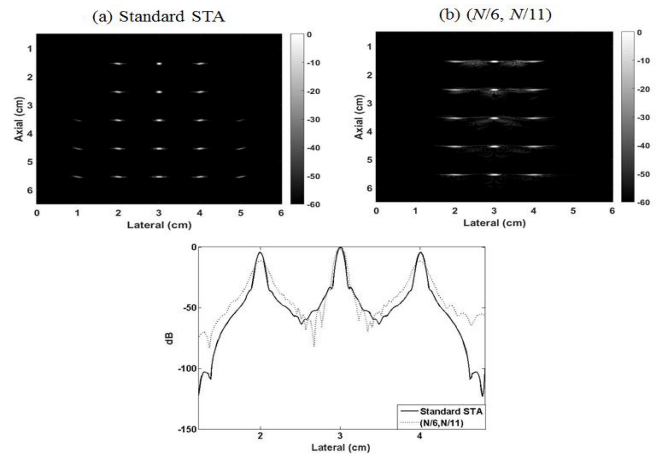


Fig. 1. Log-enveloped images obtained from various  $(n_T, n_R)$  configurations: (a)  $(N, N)$ , (b)  $(N/6, N/11)$ . Bottom row: lateral line plot at 5.5 cm depth (through the center of the point targets).

Fig. 2 shows the beamformed images of the phantom of a scattering medium with the same element combination scheme  $(n_T, n_R) = (N/6, N/11)$ . Fig. 2 (a) is the beamformed image without steering the FOV (0 degree), and (b) and (c) show the results of using REP to steer the probe array 30 degrees to the left and right, respectively. Dynamic apodization was used in all the three images when reconstructing images from the STA data. After applying the delay-REP configuration, the FOV can be steered to the symmetric positions with a comparable image quality in terms of CNR. TABLE I. shows the CNRs of the hypo-echoic inclusions at 1.5 cm, 2.5 cm and 3.5 cm, respectively along the corresponding steering angles (showing in the red circles in Fig. 2.)

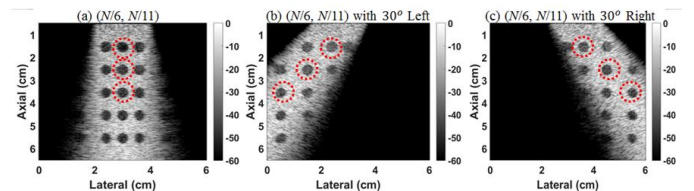


Fig. 2. Images obtained with the  $(N/6, N/11)$  configuration for various steering angles of (a)  $\theta_s = 0^\circ$ , (b)  $\theta_s = 30^\circ$  to the left, and (c)  $\theta_s = 30^\circ$  to the right.

Red circles indicate the locations of the hypo-inclusions along the steering angle, used for the calculation of CNR in TABLE I.

TABLE I. CNR measurements of the hypo-inclusions indicated by the red circles at various depths of three images in Fig. 2.

CNR	1.5cm	2.5cm	3.5cm
(a)	-3.96	-3.80	-3.84
(b)	-3.07	-3.44	-3.70
(c)	-3.10	-3.74	-3.81

#### IV. SUMMARY AND CONCLUSION

When multiple adjacent elements are combined together as one group in both transmit and receive processes, the high frame rate can be achieved due to the reduced number of transmissions. Moreover, the number of receiving channels was reduced because of combination schemes applied in the receive process as well. However, the array pitch will be increased to more than half a wavelength, which will result in the appearance of grating lobes even after the suppression due to the directivity of the group. Generally, the lateral resolution is degraded more in the region closer to the probe due to combining the probe elements, compared to the STA image from a full array.

The proposed approach can be applied in both the lateral and the elevational direction of a 2D array in the 3D ultrasound imaging. Due to the focusing in both the lateral and the elevational direction, it is expected that the image quality should be improved over the 2D imaging. Combining the adjacent elements has the potential to significantly decrease the cost of a 3D ultrasound imaging system. Alternatively, to overcome the problem of the loss in SNR of the RF signals in STA system, multiple-group excitation in one transmission can be encoded using spatial encoding methods, such as DE-STA to increase the transmit power in STA [17].

In conclusion, a high-frame rate, steerable STA system with a reduced number of receiving channels is presented. With the proposed REP configuration, the FOV can be steered. By reducing the number of measurement channels, the cost and the complexity of the imaging system can decrease due to fewer electronics associated with the array. Although the initial simulations were implemented in a 2D STA, this method can be extended to a 3D STA imaging system.

#### V. ACKNOWLEDGMENT

The authors would like to thank the following funding agencies: Natural Sciences and Engineering Research Council of Canada (NSERC), the Canada Foundation for Innovation (CFI) and Ryerson University.

#### REFERENCES

- [1] G. R. Lockwood, J. R. Talman and S. S. Brunke, "Real-time 3-D ultrasound imaging using sparse synthetic aperture beamforming," *IEEE Trans. Ultrason. Ferroelec. Freq. Contr.* 45 980–988, 1998.
- [2] J. A. Jensen, S. I. Nikolov, K. L. Gammelmark and M. H. Pedersen, "Synthetic aperture ultrasound imaging," *Ultrasonics*, vol. 44, Supplement, pp. e5-e15, 2006.
- [3] R. Y. Chiao, L. J. Thomas and S. D. Silverstein, "Sparse array imaging with spatially-encoded transmits," in *Ultrasonics Symposium Proceedings., IEEE*, vol.2, pp. 1679-1682, 1997.
- [4] R.Y. Liu, "Apparatus and method for beamforming in an ultrasonic transducer array," U.S. Patent 4 542 653, 1985.
- [5] G. R. Lockwood, P. C. Li, M. O'Donnell and F. S. Foster, "Optimizing the radiation pattern of sparse periodic linear arrays," *IEEE Trans. Ultrason., Ferroelect., Freq. Contr.*, vol. 43, pp.7-14, 1996.
- [6] R. E. Davidsen, J. A. Jensen and S. W. Smith, "Two-dimensional random arrays for real-time volumetric imaging," *Ultrason. Imag.*, vol. 16, pp. 143–163, 1994.
- [7] J. L. Schwartz and B. D. Steinberg, "Ultra sparse, ultra wide band arrays," *IEEE Trans. Ultrason., Ferroelectr., Freq. Contr.*, vol. 45, no. 2, pp. 376–393, 1998.
- [8] S. I. Nikolov and J. A. Jensen, "Application of different spatial sampling patterns for sparse array transducer design," *Ultrasonics*, vol. 37, no. 10, pp. 667–671, 2000.
- [9] J. T. Yen, J. P. Steinberg and S. W. Smith, "Sparse 2-D array design for real time rectilinear volumetric imaging," *IEEE Trans. Ultrason., Ferroelectr., Freq. Contr.*, vol. 47, no. 1, pp. 93–110, 2000.
- [10] A. Austeng and S. Holm, "Sparse 2-D arrays for 3-D phased array imaging-Design methods," *IEEE Trans. Ultrason., Ferroelect., Freq. Contr.*, vol. 49, no. 8, pp. 1073–1086, 2002.
- [11] B. Diarra, M. Robini, P. Tortoli, C. Cachard and H. Liebgott, "Design of Optimal 2-D Nongrid Sparse Arrays for Medical Ultrasound" *IEEE Transactions on Biomedical Engineering*, vol. 60, no. 11, 2013.
- [12] M. Karaman, I. O. Wygant, Ö. Oralkan and B. T. Khuri-Yakub, "Minimally Redundant 2-D Array Designs for 3-D Medical Ultrasound Imaging," *IEEE TRANSACTIONS ON MEDICAL IMAGING*, VOL. 28, NO. 7, 2009.
- [13] J. A. Johnson, M. Karaman and B. T. Khuri-Yakub, "Coherent array imaging using phased subarrays-Part I: Basic principles" , *IEEE Trans. Ultrason., Ferroelect., Freq. Contr.* , vol. 52 , no. 1 , pp.31 -50, 2005.
- [14] D. H. Turnbull and F. S. Foster, "Beam steering with pulsed two dimensional transducer arrays," *Ultrasonics, Ferroelectrics and Frequency Control, IEEE Transactions*, vol. 38, no. 4, p. 320±333, 1991
- [15] Y. Li, M. C. Kolios and Y. Xu, "Large-pitch steerable synthetic transmit aperture imaging (LPSSTA)", *Proc. SPIE. Med. Imag.*, 2016, 97901Y.
- [16] B. Savord and R. Solomon, "Fully sampled matrix transducer for real time 3D ultrasonic imaging," in *Proc. IEEE Int. Ultrasonics Symp.*, pp. 945–953, 2003.
- [17] P. Gong, M. C. Kolios and Y. Xu, "Delay-encoded transmission and image reconstruction method in synthetic transmit aperture imaging," *IEEE transactions on ultrasonics, ferroelectrics, and frequency control*, vol. 62, pp. 1745-56, 2015.
- [18] T. K. Moon and W. C. Stirling, "Mathematical Methods and Algorithms for Signal Processing," Upper Saddle, NJ:Prentice Hall, 2000.
- [19] J. A. Jensen, "Field: A program for simulating ultrasound systems," *Med. Biol. Eng. Co River mput.*, vol. 34, pp. 351-353, 1996.